

Finite Volume Evolution Galerkin Methods – A Survey

M. Lukáčová-Medvidová and K.W. Morton

*Institute of Numerical Simulation
Hamburg University of Technology, Hamburg, Germany
and Oxford University Computing Laboratory
Oxford OX1 3QD, UK*

April 17, 2009

Abstract

FVEG methods have been developed over the last dozen years to approximate unsteady hyperbolic equations in several space dimensions. In this survey the algorithmic origins of the methods are described. Then a detailed derivation of the methods is given, followed by evidence of their stability and accuracy. Finally several examples of their application are given.

1 Introduction

Finite Volume Evolution Galerkin (FVEG) methods have their origin in two main algorithmic developments, and a third technique of lesser importance. Finite element and finite volume approximations are critical starting points for the methods; and characteristic Galerkin ideas are crucial to the evolution algorithms that are used; while the third ingredient comes from the predictor-corrector schemes that are common in the approximation of ordinary differential equations. We shall concentrate on the development of FVEG methods for the approximation of systems of unsteady hyperbolic equations, though they may be used more widely; and we need to start with elliptic equations.

Finite element methods came to dominate the approximation of elliptic differential equations from the early 1970's, and their origins in engineering stress analysis can be seen much earlier. For hyperbolic equations, and particularly for unsteady problems, they have however taken much longer to make an impact. So we start with a self-adjoint, second order elliptic problem in two space dimensions posed on a polygonal domain Ω with zero boundary conditions. We seek a finite element approximation by means of triangulating the domain and constructing piecewise polynomial functions which are continuous across the triangle boundaries and satisfy the boundary conditions. It turns out that this gives an optimal approximation in a certain sense: and this objective of optimal approximation forms a guiding principle in all of the algorithmic developments that we will describe.

From our equation written in the conventional form $Lu = f$, with u the exact solution and f the data, the first step is to set up the weak form of the equation: we multiply by a test function v , integrate by parts and hence obtain the solution $u \in H_0^1(\Omega)$, the

Hilbert space of functions with square integrable first derivatives and which are zero on the boundary of the domain, given by

$$a(u, v) = (f, v) \quad \forall v \in H_0^1(\Omega), \quad (1.1)$$

where $a(\cdot, \cdot)$ is a symmetric bilinear form. If we denote by $S_0^h \subset H_0^1(\Omega)$ our *trial space* of piecewise polynomial functions, then the finite element solution $U \in S_0^h$ is given by

$$a(U, V) = (f, V) \quad \forall V \in S_0^h. \quad (1.2)$$

Then it is easy to deduce the *optimal approximation property*, in the energy norm $(a(v, v))^{1/2}$,

$$a(u - U, u - U) \leq a(u - W, u - W) \quad \forall W \in S_0^h. \quad (1.3)$$

This is the starting point from which all the powerful properties of finite element approximations are derived.

However, if the equation is not self-adjoint, and hence $a(\cdot, \cdot)$ is not symmetric, this property is lost. It can be retrieved, though, as follows. The so-called *Galerkin equations* (1.2) are generalised by use of the *Petrov-Galerkin method* in which the trial space is matched with a *test space* T_0^h , so that $U \in S_0^h$ is given by

$$a(U, V) = (f, V) \quad \forall V \in T_0^h. \quad (1.4)$$

In [2] it is shown how the test space can in principle always be matched with the trial space to retrieve the optimal approximation property. In practice this is often difficult to achieve, but a formula for the extent to which it is lost is also given in that paper.

Convection-diffusion problems are a much studied example of these situations, see [20], and also lead us towards the consideration of hyperbolic equations. A simple example is

$$-\epsilon \nabla^2 u + \nabla \cdot (\mathbf{a}u) = S, \quad (1.5)$$

in which ϵ and the components of \mathbf{a} are positive constants; in particular, we will consider the one-dimensional case. Suppose we use a piecewise linear trial space, with a typical basis function as shown on the left of Figure 1. Then appropriate test functions are *upwinded*, that is with their emphasis shifted to the left. The optimal choice is the *Hemker test function*, as shown on the right of Figure 1 for the case in which the *mesh Péclet number* is $a\Delta x/\epsilon = 20$. In the hyperbolic limit, in which the diffusion can be neglected, the test function is a piecewise constant confined to the interval upwind of the corresponding node, which corresponds to the use of the *finite volume method*.

The term finite volume method was first used to describe methods developed in the 1970's to approximate the system of hyperbolic conservation laws that model the flow of compressible fluids – see [19] and [29] for early references and [23] for a recent survey. To apply it to the convection-diffusion equation (1.5) in two dimensions, we divide the domain into a system of triangular or quadrilateral cells C_j , and take our test space T^h to consist of piecewise constants on these cells. Then, taking advantage of the fact that the equations are in conservation law form, we integrate over each cell of the mesh, apply Green's theorem to obtain a boundary flux and hence obtain the following equation for the approximation $U \in S^h$,

$$a(U, V) := \sum_j V_j \oint \left[\mathbf{a} \cdot \mathbf{n}U - \epsilon \frac{\partial U}{\partial n''} \right] dl = \int SV \, d\Omega \quad \forall V \in T^h, \quad (1.6)$$

where V_j is the value of V on C_j . Various choices for the normal derivative of the trial function “ $\partial U/\partial n$ ” are used in applications.

The convection-diffusion equation represents part of the transition from elliptic to hyperbolic problems; another crucial part is the greater emphasis on unsteady rather than steady problems. There is yet a further feature which arises from the objective of seeking a best approximation to the solution, part of the finite element viewpoint that does not arise with finite difference methods. In elliptic problems, the unknown is typically a potential, while the physically important quantity is the field given by its gradient. Thus for elliptic problems the most important approximation space is piecewise linear. However, for hyperbolic conservation laws the most important quantities are spatial integrals of the unknowns: so piecewise constant functions can play an important role in the choice of trial spaces as well as for test spaces.

Let us begin our consideration of hyperbolic problems with the following scalar, one-dimensional example,

$$\partial_t u + \partial_x f(u) \equiv \partial_t u + a(u)\partial_x u = 0. \quad (1.7)$$

Suppose that this is posed on the whole real line, with initial data $u(x, 0) = u^0(x)$ given for all x . Then its exact solution is well known: u is constant along the characteristics $dx/dt = a(u)$, which are therefore straight lines, so that

$$u(x, t) = u(x - a(u)t, 0) \quad \forall t > 0. \quad (1.8)$$

We leave on one side for the moment the possibility that the characteristics may envelope and hence give multivalued solutions at later times.

If the initial data is approximated by an expansion in local basis functions, $\{\phi_i(x)\}$, we need to define a similar expansion at later times. In the *Euler characteristic Galerkin* methods developed in [5] this is achieved as follows: from a given expansion at time $t_n = n\Delta t$, with coefficients $\{U_i^n\}$, the projection at the next time step is given by

$$(U^{n+1}, \phi_i) = \int U^n(x)\phi_i(y) dy, \quad y = x + a(U^n(x))\Delta t. \quad (1.9)$$

Representing the projection onto the space spanned by the basis functions by P_h , and the evolution step achieved through tracing the characteristics by E_Δ , this relation can be represented by the equation $U^{n+1} = P_h E_\Delta U^n$.

If, as suggested above, the basic approximation is given by an expansion in piecewise constants, it is usually desirable to have a higher order approximation before carrying out the evolution step, for example piecewise linear. This is achieved by means of a *recovery step*, denoted by R_h , for which it is important to always ensure that $P_h R_h U \equiv U$. The complete procedure for one time step can then be written

$$U^{n+1} = P_h E_\Delta R_h U^n. \quad (1.10)$$

Such *characteristic Galerkin* or, more generally, *evolution Galerkin* methods have quite a long history – see [5], [10] and [21] for references. In these references it is shown how the above formulation continues to be valid even when shock-formation takes place, so that $E_\Delta U^n$ or $E_\Delta R_h U^n$ forms an *overturned manifold*, by making use of the transport collapse operator introduced in [3].

There is a very large literature on systems of first order conservation laws in one space dimension, such as (1.7), and their numerical approximation by finite difference and finite volume methods – see [8] and [9] for references. Solutions are not always

unique and need also to satisfy an entropy condition. For numerical schemes this leads to criteria such as *entropy stability* and *TVD (Total Variation Diminishing)* conditions. The TVD properties of the FVEG schemes to be described in this paper, when applied to conservation laws of the form (1.7), have been established in [22] under natural CFL stability conditions, together with standard TVD conditions applied to the recovery stage based on discontinuous linear functions.

However, the wave equation, in two space dimensions and written as a first order system, provides the best example to introduce the methods and the problems which are the subject of this survey. Indeed, the papers [4], [27] and [28] which initiated this whole development were brought to the second author's attention when he was visiting Bangalore.

In terms of a pressure variable ϕ , and two velocity components u, v , the first order wave equation system has the form

$$\begin{aligned}\phi_t + c(u_x + v_y) &= 0, \\ u_t + c\phi_x &= 0, \quad v_t + c\phi_y = 0.\end{aligned}\tag{1.11}$$

The solution to such a system is now given by means of a characteristic cone, rather than individual characteristic lines. The classical formula is due to Kirchoff and involves integrals over the initial data in terms of a singular kernel – not a very convenient basis for a numerical algorithm. However, Butler in [4] developed a numerical scheme based on a new evolution operator, which involves integrals around the perimeter of the characteristic cone and also its curved surface, or mantle. His numerical schemes were superceded by those of [7], but the evolution operator has formed the basis of the methods developed in [11] and subsequent papers.

The various evolution-Galerkin schemes developed in this first paper used the Butler evolution operator in the same way as the one-dimensional operator based on characteristics, in a procedure of the form (1.10). However, the awkward integrals over the mantle, involving intermediate times, limit both the accuracy and the stability of the resulting schemes. Thus the final component of the FVEG schemes is the introduction of a predictor-corrector framework for the complete algorithm.

The hyperbolic systems that we shall consider are generally of the form

$$\mathbf{u}_t + \mathbf{f}_1(\mathbf{u})_x + \mathbf{f}_2(\mathbf{u})_y = 0,\tag{1.12}$$

that is, in complete conservation form. So we can apply a finite volume formulation in both space and time. The result is a cell-averaged approximation to the solution at the new time level, in terms of that at the old time level plus space-time averages over the sides of the cell. In effect, this is a predictor-corrector format. The space-time finite volume integral is the corrector step; and the Butler formulation is used in the predictor step that provides the integrals over the sides of the finite volume cells. Moreover, while the conservation form of the differential equations is appropriate for the corrector step, a characteristic form in terms of primitive rather than conserved variables, is used in the predictor step.

In the next section the detailed derivation of a second order accurate FVEG scheme is given. Its key property is that takes into account information propagated in all bicharacteristic directions. This is followed in Section 3 by evidence of the stability and accuracy of the scheme. Finally, some applications are described in Section 4 which demonstrate the accuracy with which two-dimensional wave structures are modelled.

2 Derivation of FVEG methods

From both an historical and presentational viewpoint the wave equation system (1.11) provides the most appropriate starting point for developing evolution Galerkin methods. Forming a linear combination of the equations with weights $(1, \cos \theta, -\sin \theta)$, corresponding to a bicharacteristic direction as sketched in Figure 2.1, gives

$$\frac{d}{d\sigma}(\phi - u \cos \theta - v \sin \theta) = -S. \quad (2.1)$$

The so-called source term is given by

$$S(\tilde{t}, \theta) = c[u_x(\tilde{x}, \tilde{y}, \tilde{t}) \sin^2 \theta - (u_y(\tilde{x}, \tilde{y}, \tilde{t}) + v_x(\tilde{x}, \tilde{y}, \tilde{t})) \sin \theta \cos \theta + v_y(\tilde{x}, \tilde{y}, \tilde{t}) \cos^2 \theta], \quad (2.2)$$

where $(\tilde{x}, \tilde{y}) = (x + c(t + \Delta t - \tilde{t}) \cos \theta, y + c(t + \Delta t - \tilde{t}) \sin \theta)$ and $\tilde{t} \in [t, t + \Delta t]$. Integration along the bicharacteristic then gives

$$[\phi]_Q^P - [u]_Q^P \cos \theta - [v]_Q^P \sin \theta = - \int_Q^P S(\tilde{t}, \theta) d\tilde{t}, \quad (2.3)$$

where $P = (x, y, t + \Delta t)$ and $Q = (x + c\Delta t \cos \theta, y + c\Delta t \sin \theta, t)$. Further integration over θ gives

$$\begin{aligned} \phi(P) &= \frac{1}{2\pi} \int_0^{2\pi} [\phi(Q) - u(Q) \cos \theta - v(Q) \sin \theta] d\theta \\ &\quad - \frac{1}{2\pi} \int_t^{t+\Delta t} \int_0^{2\pi} S(\tilde{t}, \theta) d\theta d\tilde{t}. \end{aligned} \quad (2.4)$$

Similarly, differently weighted combinations will give expressions for $u(P)$ and $v(P)$.

The occurrence of spatial derivatives in the source term is particularly awkward when used to evolve a piecewise constant approximation. However, an integration by parts yields the following useful lemma, see [11]:

Lemma 2.1 *Suppose $w \in C^1(\mathbb{R}^2)$, and $p \in C^1(\mathbb{R})$ is 2π -periodic. Then integrating round the circle of radius a , with a general point denoted by $Q \equiv (a \cos \theta, a \sin \theta)$, gives*

$$\int_0^{2\pi} p'(\theta) w(Q) d\theta - a \int_0^{2\pi} p(\theta) [w_x(Q) \sin \theta - w_y(Q) \cos \theta] d\theta = 0. \quad (2.5)$$

Setting $p = \sin \theta, w = u$ and $p = -\cos \theta, w = v$ with $a = c\Delta t$, and combining with a rectangle rule for the time integration, this yields the following approximate evolution formula for ϕ

$$\phi(P) := \frac{1}{2\pi} \int_0^{2\pi} [\phi(Q) - 2u(Q) \cos \theta - 2v(Q) \sin \theta] d\theta \quad (2.6)$$

with similar formulae for u and v . This is the simplest approximate evolution operator that can be derived in this way and led to a numerical algorithm called EG1.

To pursue these ideas further it is more instructive to consider a general hyperbolic system in d space variables

$$\mathbf{u}_t + \sum_{k=1}^d \mathcal{A}_k \mathbf{u}_{x_k} = 0, \quad \mathbf{x} = (x_1, \dots, x_d)^T \in \mathbb{R}^d, \quad (2.7)$$

where $\mathbf{u} = (u_1, u_2, \dots, u_m) \in \mathbb{R}^m$, with the coefficient matrices $\mathcal{A}_k \in \mathbb{R}^{(m \times m)}$. The hyperbolicity of the system implies that any matrix pencil $\mathcal{A}(\mathbf{n}) := \sum_1^d n_k \mathcal{A}_k$ has m real eigenvalues λ_j and corresponding right eigenvectors \mathbf{r}_j for any unit vector $\mathbf{n} \in \mathbb{R}^d$. In the case of constant coefficient matrices we can introduce characteristic variables $\mathbf{w} = \mathcal{R}^{-1} \mathbf{u}$, where \mathcal{R} is the matrix of right column eigenvectors corresponding to the direction \mathbf{n} . Then by multiplying the equation system from the left by \mathcal{R}^{-1} we obtain its characteristic form

$$\mathbf{w}_t + \sum_{k=1}^d \mathcal{B}_k \mathbf{w}_{x_k} = 0, \quad (2.8)$$

where $\mathcal{B}_k = \mathcal{R}^{-1} \mathcal{A}_k \mathcal{R}$. Now the key point that is exemplified by the wave equation system is that in general the coefficient matrices do not commute, so they are not all diagonalised by this transformation. Thus if we decompose \mathcal{B}_k into its diagonal part \mathcal{D}_k and its off-diagonal part \mathcal{B}'_k , we follow the derivation of [25] to obtain the following quasi-diagonalised system

$$\mathbf{w}_t + \sum_{k=1}^d \mathcal{D}_k \mathbf{w}_{x_k} = - \sum_{k=1}^d \mathcal{B}'_k \mathbf{w}_{x_k} =: \mathbf{S}. \quad (2.9)$$

It is this source term on the right that necessitates our use of the whole bicharacteristic cone to define an evolution operator, with the integrals over its mantle being particularly difficult to approximate. The simplest approximation is to apply the rectangle rule to the time integration, as in the algorithm EG1. As there, this can be integrated over the bicharacteristic direction θ in combination with the term from the foot of the characteristic; a difference in this derivation from the general theory is that there is a term evaluated at the centre $P' = (x, y, t)$ of the cone base. The resulting scheme is called EG3:

$$\phi(P) := \frac{1}{2\pi} \int_0^{2\pi} [\phi(Q) - 2u(Q) \cos \theta - 2v(Q) \sin \theta] d\theta, \quad (2.10)$$

$$u(P) := \frac{1}{2} u(P') + \frac{1}{2\pi} \int_0^{2\pi} [-2\phi(Q) \cos \theta + u(Q)(3 \cos^2 \theta - 1) + 3v(Q) \sin \theta \cos \theta] d\theta, \quad (2.11)$$

$$v(P) := \frac{1}{2} v(P') + \frac{1}{2\pi} \int_0^{2\pi} [-2\phi(Q) \sin \theta + 3u(Q) \sin \theta \cos \theta + v(Q)(3 \sin^2 \theta - 1)] d\theta. \quad (2.12)$$

We have shown in [11] that this is both more accurate and has much improved stability properties compared with the EG1 scheme.

To make further improvements to the treatment of the mantle integrals one might be tempted to turn to some form of the predictor-corrector approach. An alternative that is pursued in [13] is to consider the form of these terms for special initial data. In particular, if the initial data consists of a one-dimensional wave the resulting solution is given by the d'Alembert formula. So the mantle integrals in these cases can be calculated exactly; and the result is formulae in which the mantle integrals can be combined with those round the base of the bicharacteristic cone. For example, for piecewise constant initial data one obtains the formulae

$$\phi(P) := \frac{1}{2\pi} \int_0^{2\pi} [\phi(Q) - u(Q) \operatorname{sgn}(\cos \theta) - v(Q) \operatorname{sgn}(\sin \theta)] d\theta, \quad (2.13)$$

$$u(P) := \frac{1}{2\pi} \int_0^{2\pi} [-\phi(Q) \operatorname{sgn}(\cos \theta) + u(Q) \left(\frac{1}{2} + \cos^2 \theta\right) + v(Q) \sin \theta \cos \theta] d\theta, \quad (2.14)$$

$$v(P) := \frac{1}{2\pi} \int_0^{2\pi} [-\phi(Q) \operatorname{sgn}(\sin \theta) + u(Q) \sin \theta \cos \theta + v(Q) (\frac{1}{2} + \sin^2 \theta)] d\theta. \quad (2.15)$$

In the reference given above the following similar formulae are derived for continuous, piecewise bilinear data:

$$\phi(P) := \phi(P') + \frac{1}{4} \int_0^{2\pi} [\phi(Q) - \phi(P')] d\theta - \frac{1}{\pi} \int_0^{2\pi} [u(Q) \cos \theta + v(Q) \sin \theta] d\theta, \quad (2.16)$$

$$u(P) := u(P') - \frac{1}{\pi} \int_0^{2\pi} [\phi(Q) \cos \theta] d\theta + \frac{1}{4} \int_0^{2\pi} \left[3 (u(Q) \cos \theta + v(Q) \sin \theta) \cos \theta - u(Q) - \frac{1}{2}u(P') \right] d\theta, \quad (2.17)$$

$$v(P) := v(P') - \frac{1}{\pi} \int_0^{2\pi} [\phi(Q) \sin \theta] d\theta + \frac{1}{4} \int_0^{2\pi} \left[3 (u(Q) \cos \theta + v(Q) \sin \theta) \sin \theta - v(Q) - \frac{1}{2}v(P') \right] d\theta. \quad (2.18)$$

Note that though these formulae are only first order accurate for general data, they have been designed to be of higher accuracy for certain classes of data.

We need to introduce a recovery stage, as in the evolution-Galerkin method (1.10), and a predictor-corrector plus finite volume framework to derive a higher order accurate scheme. Such schemes have been developed in [13] and applied to a variety of problems in [13], [6], [17] – see Section 4 below; their accuracy and stability are discussed in Section 3.

Suppose then we apply a finite volume scheme to a system of hyperbolic equations in the conservation form (1.12). Using a basic piecewise constant approximation on a rectangular mesh, new cell averages $\{\mathbf{U}^{n+1}\}$ are generated from those at time level n by means of space-time averages of fluxes through the sides of the cells. It is to approximate these that we use a recovery stage and then apply the approximate evolution operators. Recovery by a continuous bilinear approximation is easily achieved by defining vertex values as simple averages of the values in the four neighbouring cells. However, such a recovered approximation would not preserve the average in each cell, which is a crucial property. Preserving these averages necessitates the use of a discontinuous bilinear approximation at the recovery stage. To complete the algorithm we need to compute the fluxes through the sides of each cell.

Altogether the FVEG method has the following predictor-corrector form

$$\begin{aligned} \mathbf{U}_{ij}^{n+1} &\approx \mathbf{U}_{ij}^n - \frac{1}{|\Omega_{ij}|} \int_{t_n}^{t_{n+1}} \int_{\partial\Omega_{ij}} \left[\mathbf{f}_1(\mathbf{U}^{*,\tau}) n_1 + \mathbf{f}_2(\mathbf{U}^{*,\tau}) n_2 \right] dS d\tau \\ \mathbf{U}^{*,\tau} &\approx E_\tau(R_h \mathbf{U}^n). \end{aligned} \quad (2.19)$$

Here we have used a standard notation: \mathbf{U}^n is an approximate solution at t_n , $t_n = n\Delta t$, $|\Omega_{ij}|$ denotes the area of a finite volume Ω_{ij} having an outer normal $\mathbf{n} := (n_1, n_2)$ and $\mathbf{U}^{*,\tau}$ is the solution predicted at cell interfaces by the approximate evolution operator E_τ . In the FVEG schemes referred to above these space-time integrals are approximated by the mid-point rule in time and various quadrature formulae in space – the midpoint rule, the trapezoidal rule and Simpson's rule.

The stability and accuracy properties of these choices will be discussed in Section 3. The results given in [13] and [16] show that both accuracy and stability depend on how the recovery stage is implemented. Indeed, the approximate evolution operator (2.13)–(2.15) applied on piecewise constant data, i.e. $R_h = Id$ in (2.19), yields the first order FVEG scheme. In order to obtain second order accuracy we need to employ a bilinear recovery. Using the evolution operator (2.16)–(2.18) and the continuous piecewise bilinear recovery R_h^C yields a second order FVEG scheme, denoted by FVEG-B in [13]. As already mentioned above such a recovery does not preserve the cell averages. As a consequence this yields the reduced stability as well as accuracy of the FVEG-B scheme [13]. The best scheme, denoted by Scheme A in [13], applies (2.16)–(2.18) to the continuous bilinear recovered approximation and (2.13)–(2.15) to the piecewise constant approximation that maintains the conservation property. Then the predictor step in (2.19) reads

$$U^{*,\tau} \approx E_\tau^{bilin} R_h^C U^n + E_\tau^{const} (1 - \mu_x^2 \mu_y^2) U^n, \quad (2.20)$$

where E_τ^{const} and E_τ^{bilin} denote the approximate evolution operators (2.13)–(2.15) and (2.16)–(2.18), respectively, and μ_x, μ_y are the standard averaging difference operators in x - and y -directions. Where below we refer to the FVEG scheme we shall mean the above choice.

3 Accuracy and stability

For any numerical scheme fundamental theoretical questions concern its stability and accuracy. These topics were particularly important for the development of FVEG schemes and have been investigated in [12], [13], [16] as well as in [18]. In this section we will briefly summarize the main results and point out some open questions.

3.1 Error analysis

In [12] the *accuracy* of the FVEG scheme for a linearized, constant coefficient system of hyperbolic conservation laws in two-dimensions has been investigated. Let us rewrite the FVEG scheme in the following compact form

$$U^{n+1} = \mathcal{N}_h R_h U^n, \quad (3.1)$$

where \mathcal{N}_h denotes the FVEG update (2.19) and R_h is a conservative piecewise bilinear recovery. Further, let Q be the L^2 -projection given by integral averages onto a space S_h^0 of piecewise constant step functions,

$$Q\mathbf{u} = \sum_{i,j \in \mathbb{Z}} \left(\frac{1}{h^2} \int_{\Omega_{ij}} \mathbf{u}(x, y) dx dy \right) \chi_{ij} \quad \mathbf{u} \in (L^2(\mathbb{R}^2))^m, \quad (3.2)$$

where χ_{ij} is the characteristic function for the square mesh cell Ω_{ij} . Denote by $\|\cdot\|$ the L^2 -norm. The global error between the exact solution \mathbf{u} and the approximate solution \mathbf{U} is then defined as

$$\mathbf{e}^{n+1} := \mathbf{u}(\cdot, t_{n+1}) - R_h \mathbf{U}^{n+1}.$$

The error can be decomposed into a projection error $\boldsymbol{\eta}$ and an evolutionary error $\boldsymbol{\xi}$:

$$\mathbf{e}^{n+1} = (\mathbf{u}(t_{n+1}) - R_h Q \mathbf{u}(t_{n+1})) + (R_h Q \mathbf{u}(t_{n+1}) - R_h \mathbf{U}^{n+1}) \equiv \boldsymbol{\eta}^{n+1} + \boldsymbol{\xi}^{n+1}. \quad (3.3)$$

Firstly, it is clear, that the projection error onto piecewise bilinear functions is of second order, i.e. $\|\boldsymbol{\eta}^{n+1}\| \leq ch^2$. Now we derive an evolution equation for $\boldsymbol{\xi}$ by introducing the term $R_h\mathcal{N}_hR_hQ\mathbf{u}$ as follows,

$$\boldsymbol{\xi}^{n+1} = R_h(Q\mathbf{u}(t_{n+1}) - \mathcal{N}_hR_hQ\mathbf{u}(t_n)) + (R_h\mathcal{N}_hR_hQ\mathbf{u}(t_n) - R_h\mathcal{N}_hR_h\mathbf{U}^n). \quad (3.4)$$

We need to show that the operator $R_h\mathcal{N}_h$ is strongly stable, i.e.

$$\|R_h\mathcal{N}_h\| \leq 1. \quad (3.5)$$

This question has been studied in particular for constant coefficient systems, e.g. the wave equation system in [16]. It has been proved that the approximate evolution operator (2.13)-(2.15) derived in [13] yields an FVEG method having a natural stability limit of CFL=1.

Now it is clear from the strong stability condition (3.5) that the evolutionary error $\boldsymbol{\xi}^{n+1}$ is in fact determined only by the recovered truncation error

$$\mathbf{T}^n := \frac{1}{\Delta t}(Q\mathbf{u}(t_{n+1}) - \mathcal{N}_hR_hQ\mathbf{u}(t_n)), \quad (3.6)$$

through the recurrence relation $\|\boldsymbol{\xi}^{n+1}\| \leq \|\boldsymbol{\xi}^n\| + \Delta t\|R_h\mathbf{T}^n\|$. This yields

$$\|\boldsymbol{\xi}^{n+1}\| \leq \|\boldsymbol{\xi}^0\| + \Delta t \sum_{j=0}^n \|R_h\mathbf{T}^j\|.$$

In [12] we have proved that $\|\mathbf{T}^j\| = \mathcal{O}(\Delta t^2)$, which implies second order accuracy for the FVEG scheme based on bilinear recovery. The stability of such schemes is discussed in the next section.

Table 1 presents the experimental order of convergence and confirms second order accuracy of two FVEG schemes. For a smooth solution of the wave equation system we have compared the accuracy of the rotated Richtmyer Lax-Wendroff scheme (LW) with an FVEG scheme using the EG3 approximate evolution operator (2.10)-(2.12), denoted by FVEG3, as well as the second order FVEG scheme. We have set the CFL number to 0.9 for the FVEG scheme and for the Lax-Wendroff scheme; for the FVEG3 scheme only the CFL=0.55 has been used due to the reduced stability range. The final time was set to $T = 10$.

We can clearly see much better accuracy of both FVEG schemes in comparison to the Lax-Wendroff scheme; the FVEG scheme is at least 5 times more accurate than the standard finite difference method. We should point out that the superior accuracy of the FVEG scheme in comparison to standard dimensional splitting schemes is even more crucial for nonlinear systems, cf. Figure 4.4.

3.2 Stability and entropy stability

Stability of the FVEG schemes has been investigated theoretically as well as experimentally for a linear two-dimensional wave equation system by the von-Neumann analysis in [16], [13]. Using the Fourier transformation we have derived in [16] amplification matrices for the first and second order FVEG schemes applied to the wave equation system (1.11). In order to evaluate their spectral radius the standard matlab routine has been used. We have shown that the first order FVEG scheme based on (2.13)-(2.15) is stable up to CFL=1.00 if the trapezoidal rule is used for flux integration along cell interfaces. If the

N	FVEG	FVEG3	LW
20	0.386944	1.419723	1.294829
40	0.087802	0.335918	0.383314
80	0.021017	0.062675	0.098100
160	0.005196	0.013484	0.024551
EOC	2.02	2.22	1.99

Table 1: Accuracy test, giving the error $\|\mathbf{u}(T) - \mathbf{U}^n\|$ for the FVEG schemes on grids with $N \times N$ mesh cells.

Simpson rule is used instead the stability limit is CFL=0.75. Integrals along the sonic circle, i.e. the base of bicharacteristic cone, are computed exactly for given piecewise smooth data. For the second order FVEG method the stability limit using the trapezoidal quadrature is slightly reduced to CFL=0.94. If the Simpson rule is used to evaluate cell interface integrals in the second order FVEG method the stability limit remains at CFL=0.75. We note that for the FVEG3 the stability limit was only CFL=0.56. It is the approximate evolution operators (2.13)-(2.15) and (2.16)-(2.18) representing one-dimensional planar waves exactly that yield the improved stability ranges of the FVEG schemes.

For nonlinear hyperbolic conservation laws weak solutions might be non-unique and the entropy inequality has to be used in order to pick up a physically relevant solution. In [18] the *entropy stability* of the semi-discrete FVEG scheme, cf. (3.10)-(3.12), has been investigated for one-dimensional hyperbolic conservation laws. Following Tadmor [30, 31] we study the entropy stability of this FVEG scheme using the comparison approach with the so-called entropy conservative scheme. Since the numerical viscosity of the entropy conservative scheme is known explicitly, see [30], we need to compute the numerical viscosity of the FVEG scheme and show that it is larger than or equal to that of the entropy conservative scheme. This implies directly the entropy stability of the FVEG scheme. As a consequence a semi-discrete form of the cell entropy inequality is fulfilled:

$$\frac{d}{dt}U(\mathbf{u}_\nu(t)) + \frac{F_{\nu+\frac{1}{2}} - F_{\nu-\frac{1}{2}}}{\Delta x_\nu} \leq 0, \quad (3.7)$$

here $U(\mathbf{u})$ is the convex entropy function and $F_{\nu+\frac{1}{2}} := F(\mathbf{u}_\nu(t), \mathbf{u}_{\nu+1}(t))$ is the corresponding consistent entropy flux function.

Now let us consider a one-dimensional hyperbolic system with a symmetric Jacobian matrix \mathcal{A} and use the orthogonal shock-based Riemann path $\{\mathbf{u}_+^j\}_{j=1,\dots,N+1}$ that connects two neighbouring discrete states \mathbf{u}_ν and $\mathbf{u}_{\nu+1}$. Thus we resolve the interface through a series of shocks and have

$$\mathbf{f}(\mathbf{u}_+^{j+1}) - \mathbf{f}(\mathbf{u}_+^j) = s_+^j (\mathbf{u}_+^{j+1} - \mathbf{u}_+^j), \quad j = 1, \dots, N. \quad (3.8)$$

Let us denote by \mathbf{r}_+^j , $j = 1, 2, \dots, N$, unit vectors in the direction of the intermediate states \mathbf{u}_+^j , i.e. $\mathbf{r}_+^j := (\mathbf{u}_+^{j+1} - \mathbf{u}_+^j) / |\mathbf{u}_+^{j+1} - \mathbf{u}_+^j|$. Further, let $\{\boldsymbol{\ell}_+^j\}_{j=1,\dots,N}$ be the corresponding orthogonal system to $\{\mathbf{r}_+^j\}_{j=1,\dots,N}$, i.e. $\langle \mathbf{r}_+^j, \boldsymbol{\ell}_+^k \rangle = \delta_{jk}$. Denote the wave strengths along the sub-paths by α_+^j

$$\alpha_+^j := \langle \boldsymbol{\ell}_+^j, \mathbf{u}_{\nu+1} - \mathbf{u}_\nu \rangle. \quad (3.9)$$

To guarantee the entropy stability of the FVEG scheme we employ the numerical flux

$$\mathbf{H}_{\nu+\frac{1}{2}} = \mathbf{H}(\mathbf{u}_\nu, \mathbf{u}_{\nu+1}) := \mathbf{f}(\mathbf{u}_+^*) - \mathcal{J}_+, \quad (3.10)$$

which involves the intermediate state \mathbf{u}_+^* predicted by the approximate evolution operator. Indeed, for one-dimensional systems bicharacteristics reduce to characteristics and we can interpret the evolution operator as

$$\mathbf{u}_+^* := \mathbf{u}_\nu + \sum_{\{j: s_+^j \leq 0\}} \alpha_+^j \mathbf{r}_+^j. \quad (3.11)$$

In order to guarantee the entropy stability we add an entropy correction term \mathcal{J}_+ , that is given by

$$\mathcal{J}_+ := \frac{\kappa}{2} \sum_{j=1}^N [\lambda_+^j]^+ \alpha_+^j \mathbf{r}_+^j, \quad [\lambda_+^j]^+ = \max\{\lambda_+^j, 0\}. \quad (3.12)$$

Here, κ is an amplitude to be tuned later on, and $[\lambda_+^j]^+$ is the *positive part* of the jumps in eigenvalues along the sub-paths

$$[\lambda_+^j] := \lambda^j(\mathcal{A}(\mathbf{u}_+^{j+1})) - \lambda^j(\mathcal{A}(\mathbf{u}_+^j)). \quad (3.13)$$

First we need to specify the numerical viscosity of the FVEG scheme (3.10), see [18].

Lemma 3.1 *The FVEG scheme (3.10) admits in one space-dimension the following viscosity form*

$$\begin{aligned} \frac{d}{dt} \mathbf{u}_\nu(t) &= -\frac{1}{2\Delta x_\nu} \left[\mathbf{f}(\mathbf{u}_{\nu+1}) - \mathbf{f}(\mathbf{u}_{\nu-1}) \right] \\ &+ \frac{1}{2\Delta x_\nu} \left[\sum_{j=1}^N q_+^{j+\frac{1}{2}} \alpha_+^j \boldsymbol{\ell}_+^j - \sum_{j=1}^N q_-^{j+\frac{1}{2}} \alpha_-^j \boldsymbol{\ell}_-^j \right] \end{aligned} \quad (3.14)$$

with viscosity coefficients

$$q_+^j = |s_+^j| + \kappa [\lambda_+^j]^+.$$

Using this result it can be shown, cf. [18], that if the viscosity parameter $\kappa \geq 1/4$ then $q_+^j \geq q_+^{j,*}$, where $q_+^{j,*}$ is the numerical viscosity of the entropy conservative scheme¹. We should point out that the entropy correction term \mathcal{J} is indeed necessary in order to obtain entropy stability of the FVEG scheme. If it is not used, i.e. $\kappa = 0$, then the scheme can produce solutions violating entropy inequality. The concept presented in [18] can be generalized to nonsymmetric hyperbolic systems easily, see [30]. Applying dimensional splitting a generalization to multidimensional systems can be developed, too.

In order to demonstrate the influence of entropy correction term \mathcal{J} let us consider a well-known dam break test [9]. The so-called shallow water system, cf. (4.4), models the wave propagation of two uniform water levels, both at rest initially, separated by a wall at $x = 0$

$$\begin{aligned} h &= 0.1, & u &= 0, & |x| &\geq 0, \\ h &= 1, & u &= 0, & |x| &< 0. \end{aligned} \quad (3.15)$$

¹To be more precise we can show that the inequality holds in the leading order terms, i.e. $q_+^{j,*} \leq q_+^j + c|\mathbf{u}_{\nu+1} - \mathbf{u}_\nu|^2$.

We approximate the shallow water system by the first and second order FVEG scheme, cf. (2.19), (2.20) and (4.7)-(4.8), [17]. After the wall collapses the solution exhibits the left propagating depression wave (rarefaction) and the right propagating bore (shock). Within the depression wave there is a critical point, where the Froude number $Fr := |\mathbf{u}|/c = 1$. Many numerical schemes that are based on the solution of a linearized Riemann problem yield an incorrect entropy glitch at the critical point. It is the small discontinuity jump, unphysical entropy violating shock, within the depression wave. This can be seen very well also in our experiments, see Figures 3.1, 3.2 for the first and second order FVEG method, respectively. Here we have plotted the water depth h as well as the Froude number Fr for the first and second order FVEG schemes, respectively. In the second order method the minmod limiter was used, cf. [9]. If the entropy correction term \mathcal{J} has been added we obtain correct resolution of the rarefaction wave.

4 Applications

The aim of this section is to demonstrate robustness, good multidimensional behaviour, high accuracy, stability and efficiency of the FVEG schemes through a series of numerical experiments. In order to illustrate the flexibility of the FVEG scheme we present applications to different systems of conservation laws; the nonlinear Euler equations of gas dynamics, the shallow water equations with bottom topography and the wave equation with a discontinuous wave speed.

4.1 Euler equations

A classic example of hyperbolic conservation laws arises from gas dynamics. Conservation of mass, momentum and energy of an inviscid compressible fluid is governed by the so-called Euler equations. The finite volume formulation that automatically implies the conservation property, works with the conservation form of the Euler equations

$$\mathbf{u}_t + \mathbf{f}_1(\mathbf{u})_x + \mathbf{f}_2(\mathbf{u})_y = 0, \quad (4.1)$$

where the vector of conservative variables and the fluxes are

$$\mathbf{u} := \begin{pmatrix} \rho \\ \rho u \\ \rho v \\ e \end{pmatrix}, \quad \mathbf{f}_1(\mathbf{u}) := \begin{pmatrix} \rho u \\ \rho u^2 + p \\ \rho uv \\ (e + p)u \end{pmatrix}, \quad \mathbf{f}_2(\mathbf{u}) := \begin{pmatrix} \rho v \\ \rho uv \\ \rho v^2 + p \\ (e + p)v \end{pmatrix}.$$

Here e stands for the total energy, i.e. $e = p/(\gamma - 1) + \rho(u^2 + v^2)/2$. In order to evaluate fluxes along cell interfaces in the FVEG scheme (2.19) we need to evaluate integrals along the cell interface and around the Mach cone. There are generally two possibilities to do this; integrals can either be evaluated exactly or by means of a suitable numerical quadrature. The favoured approach with respect to stability and accuracy is to use exact integration around the Mach cone and numerical integration of fluxes along cell interfaces. For the latter the Simpson rule and the trapezoidal rule has been used in order to take multidimensional corner effects into account. The midpoint rule would reduce the FVEG

scheme to a standard dimensional splitting FVM. However, we should point out that for problems with non-zero advection velocities the use of the trapezoidal rule would yield an unconditionally unstable method, see [13]; so we use in what follows the Simpson rule to integrate cell interface fluxes.

Applying the general procedure as described in the Section 2 the following exact integral equations can be derived for the locally linearized system of Euler equations around the state $(\bar{u}, \bar{v}, \bar{c})$, where (\bar{u}, \bar{v}) denotes the velocity vector and \bar{c} is the wave speed $\bar{c} := \gamma \bar{p} / \bar{\rho}$, see [13]. Evolution takes place along the bicharacteristic cone, see Figure 4.1. Here $P = (x, y, t_n + \tau)$ is the peak of the bicharacteristic cone, $P' = (x - \bar{u}\tau, y - \bar{v}\tau, t_n)$ denotes the center of the sonic circle at time t_n , $\tilde{P}' = (x - \bar{u}(t_n + \tau - \tilde{t}), y - \bar{v}(t_n + \tau - \tilde{t}), \tilde{t})$, $\tilde{Q} = (x - \bar{u}(t_n + \tau - \tilde{t}) + \bar{c}(t_n + \tau - \tilde{t}) \cos \theta, y - \bar{v}(t_n + \tau - \tilde{t}) + \bar{c}(t_n + \tau - \tilde{t}) \sin \theta, \tilde{t})$ denotes an arbitrary point on the mantle and $Q(\theta) = Q(\theta, \tilde{t})|_{\tilde{t}=t_n}$ is a point at the perimeter of the sonic circle at time t_n . Thus we have

$$\begin{aligned} \rho(P) &= \rho(P') - \frac{p(P')}{\bar{c}^2} + \frac{1}{2\pi} \int_0^{2\pi} \left[\frac{p(Q)}{\bar{c}^2} - \frac{\bar{\rho}}{\bar{c}} (u(Q) \cos \theta + v(Q) \sin \theta) \right] d\theta \\ &\quad - \frac{\bar{\rho}}{\bar{c}} \frac{1}{2\pi} \int_0^{2\pi} \int_{t_n}^{t_n + \tau} S(\tilde{Q}) d\tilde{t} d\theta, \end{aligned} \quad (4.2)$$

$$\begin{aligned} u(P) &= \frac{1}{2\pi} \int_0^{2\pi} \left[-\frac{p(Q)}{\bar{\rho}\bar{c}} \cos \theta + (u(Q) \cos \theta + v(Q) \sin \theta) \cos \theta \right] d\theta \\ &\quad + \frac{1}{2\pi} \int_0^{2\pi} \int_{t_n}^{t_n + \tau} S(\tilde{Q}) \cos \theta d\tilde{t} d\theta + \frac{1}{2} u(P') - \frac{1}{2\bar{\rho}} \int_{t_n}^{t_n + \tau} p_x(\tilde{P}') d\tilde{t}, \end{aligned} \quad (4.3)$$

where the so-called source term S that arises from multidimensionality of the system is given analogously to (2.2) by

$$S(\theta, \tilde{t}) := \bar{c} [u_x(\theta, \tilde{t}) \sin^2 \theta - (u_y(\theta, \tilde{t}) + v_x(\theta, \tilde{t}) \sin \theta \cos \theta + v_y(\theta, \tilde{t}) \cos^2 \theta)].$$

Similar equations hold for the y -velocity v and pressure p .

Now, the crucial step for stability as well as accuracy of the FVEG scheme is the approximation of the mantle integrals, i.e. the time integrals from t_n to $t_n + \tau$ in the above integral equations. Applying approximations analogous to (2.13)-(2.15) we derive approximate evolution operators for the Euler equations with the CFL number close to a natural stability limit of CFL=1. In what follows we present the approximate evolution operator for piecewise constant data; in a similar way the approximate evolution operator for higher order polynomials can be derived, too, cf. [13].

$$\begin{aligned} \rho(P) &:= \rho(P') - \frac{p(P')}{\bar{a}^2} \\ &\quad + \frac{1}{2\pi} \int_0^{2\pi} \left[\frac{p(Q)}{\bar{c}^2} - \frac{\bar{\rho}}{\bar{c}} (u(Q) \operatorname{sgn}(\cos \theta) + v(Q) \operatorname{sgn}(\sin \theta)) \right] d\theta, \\ u(P) &:= \frac{1}{2\pi} \int_0^{2\pi} \left[-\frac{p(Q)}{\bar{\rho}\bar{c}} \operatorname{sgn}(\cos \theta) + u(Q) \left(\frac{1}{2} + \cos^2 \theta \right) + v(Q) \sin \theta \cos \theta \right] d\theta \end{aligned}$$

with analogous formulae for v and p .

Problem 1. In this example we would like to demonstrate good multidimensional behavior of the FVEG scheme by solving the well-known Sod-2D test problem with discontinuous initial data

$$\begin{aligned} \rho = 1, \quad u = 0, \quad v = 0, \quad p = 1, & \quad \|\mathbf{x}\| < 0.4, \\ \rho = 0.125, \quad u = 0, \quad v = 0, \quad p = 0.1, & \quad \text{else.} \end{aligned}$$

We consider this initial-value problem as a cylindrical explosion problem. The computational domain is a square $[-1, 1] \times [-1, 1]$. The mesh is uniform square, and initial data are implemented by taking the integral average on each cell, i.e., by projecting them onto a piecewise constant function in S_h^0 . We set the CFL number to 0.7 and take a mesh with 400×400 cells.

The solution exhibits a circular shock travelling away from the center, a circular contact discontinuity travelling in the same direction, and a circular rarefaction wave travelling towards the origin at $(0, 0)$. Within the rarefaction fan, a secondary shock is created; it travels inwards and focuses at the origin creating a peak in pressure and density at time $T = 1.7$. In Figures 4.2, 4.3 we have plotted three-dimensional graphs of density at $T = 0.2$ and $T = 1.7$ as well as two-dimensional graph of isolines at time $T = 0.2$, respectively. Both results were obtained by the second order FVEG scheme and demonstrate good multidimensional resolution of all significant structures.

4.2 Shallow water equations

Shallow water equations with a source term modelling bottom topography arise in many geophysical models; for example in oceanography, river flow engineering or climatology. Written in the conservation form they are given as

$$\mathbf{u}_t + \mathbf{f}_1(\mathbf{u})_x + \mathbf{f}_2(\mathbf{u})_y = \mathbf{b}(\mathbf{u}), \quad (4.4)$$

where

$$\begin{aligned} \mathbf{u} &= \begin{pmatrix} h \\ hu \\ hv \end{pmatrix}, \quad \mathbf{f}_1(\mathbf{u}) = \begin{pmatrix} hu \\ hu^2 + \frac{1}{2}gh^2 \\ huv \end{pmatrix}, \\ \mathbf{f}_2(\mathbf{u}) &= \begin{pmatrix} hv \\ huv \\ hv^2 + \frac{1}{2}gh^2 \end{pmatrix}, \quad \mathbf{b}(\mathbf{u}) = \begin{pmatrix} 0 \\ -ghb_x \\ -ghb_y \end{pmatrix}. \end{aligned}$$

Here h denotes the water depth, u, v are vertically averaged velocity components in the x - and y -directions, g stands for the gravitational constant and $b = b(x, y)$ denotes the bottom topography. The wave speed is given as $c := \sqrt{g/h}$.

This system belongs to the class of hyperbolic balance laws. For such problems the goal is to derive a scheme that automatically preserves some physically relevant equilibrium states. Equilibrium solutions play an important role because they are obtained usually as a limit when time tends to infinity. The scheme preserving equilibrium states exactly or at least with high accuracy is called *well-balanced*. Our aim in this section is to show how to include physical source terms in the framework of evolution operators and approximate them in such a way that they are preserved exactly. In particular, we will concentrate on the lake at rest equilibrium state, i.e. $(h + b)_x = 0$, $(h + b)_y = 0$ and $u = 0 = v$.

Applying a general procedure for the derivation of exact integral equations for linearized systems as described in Section 2 we obtain

$$\begin{aligned}
h(P) &:= \frac{1}{2\pi} \int_0^{2\pi} h(Q) - \frac{\bar{c}}{g} (u(Q) \cos \theta + v(Q) \sin \theta) d\theta - \frac{1}{2\pi} \int_0^{2\pi} \int_{t_n}^{t_n+\tau} \frac{\bar{c}}{g} S(\tilde{Q}) d\theta d\tilde{t} \\
&\quad + \frac{1}{2\pi} \bar{c} \int_0^{2\pi} \int_{t_n}^{t_n+\tau} (b_x(\tilde{Q}) \cos \theta + b_y(\tilde{Q}) \sin \theta) d\theta d\tilde{t}, \tag{4.5}
\end{aligned}$$

$$\begin{aligned}
u(P) &:= \frac{1}{2} u(P') + \frac{1}{2\pi} \int_0^{2\pi} -\frac{g}{\bar{c}} h(Q) \cos \theta + u(Q) \cos^2 \theta + v(Q) \sin \theta \cos \theta d\theta \\
&\quad - \frac{g}{2} \int_{t_n}^{t_n+\tau} (h_x(\tilde{P}') + b_x(\tilde{P}')) d\tilde{t} + \frac{1}{2\pi} \int_0^{2\pi} \int_{t_n}^{t_n+\tau} S(\tilde{Q}) \cos(\theta) d\theta d\tilde{t} \\
&\quad - \frac{g}{2\pi} \int_0^{2\pi} \int_{t_n}^{t_n+\tau} (b_x(\tilde{Q}) \cos^2 \theta + b_y(\tilde{Q}) \sin \theta \cos \theta) d\theta d\tilde{t}. \tag{4.6}
\end{aligned}$$

An analogous equation holds for the second velocity v . Evolution takes place along the bicharacteristic cone; here we use a similar notation as in the previous section.

In order to obtain the *well-balanced* approximation of source terms it is important to represent all terms arising in the equilibrium condition by the same integrals. For the lake at rest state it is in particular important to approximate the total water surface $h + b$ in the same way. This is the main idea of the well-balanced evolution operators. Then approximating mantle integrals in such a way that one-dimensional waves are computed exactly, cf. Section 2, we obtain after some calculation the following well-balanced approximate evolution operator for piecewise constant approximate functions

$$\begin{aligned}
h(P) &:= -b(P) + \frac{1}{2\pi} \int_0^{2\pi} (h(Q) + b(Q)) - \frac{\bar{c}}{g} (u(Q) \operatorname{sgn}(\cos \theta) + v(Q) \operatorname{sgn}(\sin \theta)) d\theta \\
&\quad + \frac{\tau}{2\pi} \int_0^{2\pi} (\bar{u} b_x(Q) + \bar{v} b_y(Q)) d\theta, \tag{4.7}
\end{aligned}$$

$$\begin{aligned}
u(P) &:= \frac{1}{2\pi} \int_0^{2\pi} \left(-\frac{g}{\bar{c}} (h(Q) + b(Q)) \operatorname{sgn}(\cos \theta) + u(Q) \left(\cos^2 \theta + \frac{1}{2} \right) \right. \\
&\quad \left. + v(Q) \sin \theta \cos \theta \right) d\theta. \tag{4.8}
\end{aligned}$$

One can easily check that if $h + b = \text{const.}$ and $u = 0 = v$ at time t_n then the same property holds also at t_{n+1} . The well-balanced approximate evolution operator is used in the finite volume update in order to evaluate fluxes along cell-interfaces. Note that in order to keep a delicate balance between sources and fluxes the source terms have to be approximated in a suitable way in the finite volume update, too. This is done using the interface-based approach, i.e. $hb_x \approx \mu_x h^* \delta_x b$, where h^* denotes the predicted solution at cell interfaces obtained by the approximate evolution operator and μ_x, δ_x are the standard averaging and central difference operators.

Problem 2. The aim of this experiment is to demonstrate preservation of a stationary steady state. The bottom topography consists of one hump

$$b(x) = \begin{cases} 0.25(\cos(10\pi(x - 0.5)) + 1) & \text{if } |x - 0.5| < 0.1 \\ 0 & \text{otherwise} \end{cases}$$

and the initial data are $u(x, 0) = 0$, $h(x, 0) = 1 - b(x)$. Note that this is an equilibrium state. The computational domain is the interval $[0, 1]$. It should be pointed out that the one-dimensional problems are actually computed by a two-dimensional code by imposing zero tangential velocity $v = 0$. In Table 2 the L^1 -errors for different times computed with the first order FVEG method and with the second order FVEG method are presented. Although we have used a rather coarse mesh consisting of 20×20 mesh cells, it can be seen clearly that the FVEG scheme balances up to the machine accuracy also for long time computations.

Table 2: The L^1 -error of the well-balance FVEG scheme using 20×20 mesh cells.

Method	$t = 0.2$	$t = 1$	$t = 10$
first order FVEG	1.11×10^{-17}	7.21×10^{-17}	1.33×10^{-16}
second order FVEG	2.77×10^{-17}	5.55×10^{-17}	4.44×10^{-17}

In the next experiment we want to illustrate the high efficiency of the FVEG scheme. We used smooth initial data for all components of solution as well as for bottom topography and computed the solution for a short time instance having still a smooth solution. Now the computational domain $[0, 1] \times [0, 1]$ was consecutively divided into 25, 50, \dots , 800 mesh cells in each direction. We have compared solutions obtained by the second order FVEG scheme as well as by the second order and fourth order well-balanced FVM. For the second order well-balanced FVM of Noelle et al. [24] the second order Runge-Kutta method was used for time integration, the third order Gaussian quadrature was used for cell-interface integrals of fluxes and the second order WENO recovery was applied. The reference solution was obtained by the fourth order well-balanced FV method, cf. [24].

Figure 4.4 illustrates the CPU/accuracy behaviour graphically. On the left of Figure 4.4 a comparison between the second order FVEG and FV methods are presented, whereas on the right we show the comparison between the fourth order well-balanced FVM of Noelle [24] and the second order FVEG scheme. The FVEG schemes yields on coarse meshes still more accurate solutions. In fact, for meshes up to approximately 100×100 cells, which are often used for practical computations, it is more efficient to use the second order FVEG scheme than the fourth order FVM. Let us point out that high accuracy of the FVEG scheme in comparison to standard dimensional-splitting FV methods is a general phenomenon that has been observed for different hyperbolic conservation laws. We believe that the main reason for such a property is the fact that evolution operators take all infinitely many directions of wave propagations into account explicitly.

4.3 Wave propagation in heterogeneous media

The aim of this section is to present a generalization of the finite volume evolution Galerkin scheme for hyperbolic systems with spatially varying flux functions. We will illustrate our methodology for acoustic waves in a heterogeneous medium but the results can be generalized to more complex systems. Written in the conservation form the wave equation system with spatially varying wave speed reads

$$\mathbf{u}_t + (\mathbf{f}_1(\mathbf{u}))_x + (\mathbf{f}_2(\mathbf{u}))_y = 0, \quad (4.9)$$

where

$$\mathbf{u} = \begin{bmatrix} p \\ \rho_0 u \\ \rho_0 v \end{bmatrix}, \quad \mathbf{f}_1(\mathbf{u}) = \begin{bmatrix} c_0^2 \rho_0 u \\ p \\ 0 \end{bmatrix}, \quad \mathbf{f}_2(\mathbf{u}) = \begin{bmatrix} c_0^2 \rho_0 v \\ 0 \\ p \end{bmatrix}. \quad (4.10)$$

Here $c_0 = \sqrt{\gamma p_0 / \rho_0}$, which is not constant, denotes the wave speed, p_0 and ρ_0 denote for the background pressure and density, respectively.

The envelope of bicharacteristics passing through a fixed point in space-time creates in general the so-called characteristic conoid, see Figure 4.5. Time evolution of the normal vector $\mathbf{n}(\theta(t))$ and of points $(x(t), y(t))$ belonging to the mantle of the characteristic conoid can be described by means of the extended lemma on bicharacteristics [26]

$$\begin{aligned} \frac{dx}{dt} &= -c_0(x, y) \cos \theta, & \frac{dy}{dt} &= -c_0(x, y) \sin \theta, & \frac{d\theta}{dt} &= -c_{0x} \sin \theta + c_{0y} \cos \theta, \\ \frac{dx}{dt} &= 0, & \frac{dy}{dt} &= 0, & \frac{d\theta}{dt} &= 0, \\ \frac{dx}{dt} &= c_0(x, y) \cos \theta, & \frac{dy}{dt} &= c_0(x, y) \sin \theta, & \frac{d\theta}{dt} &= c_{0x} \sin \theta - c_{0y} \cos \theta, \quad \theta \in [0, 2\pi]. \end{aligned} \quad (4.11)$$

Note that for the wave equation system with constant wave speed $c_0(x, y) \equiv \text{const.}$ the bicharacteristic equations (4.11) can be solved immediately to get the bicharacteristics to be straight lines and the characteristic conoid reduces to the bicharacteristic cone, see Figure 4.1.

Since the system (4.10) is linear we can derive the exact integral equations without any linearization of the wave speed. As described above we transform the wave equation system to a system in characteristic variables, split the Jacobians into the diagonal and off-diagonal part and integrate from t_n to t_{n+1} along $(x(t), y(t), \theta(t))$. Transformation back to the physical variables and suitable manipulations yield the following exact integral equations, cf. [1],

$$\begin{aligned} p(P) &= \frac{1}{2\pi} \int_0^{2\pi} (p - z_0 u \cos \theta - z_0 v \sin \theta) (Q) d\omega \\ &\quad - \frac{1}{2\pi} \int_0^{2\pi} \int_{t_n}^{t_n+\tau} (z_0 (c_{0x} u + c_{0y} v)) (\tilde{Q}) d\tilde{t} d\omega \\ &\quad - \frac{1}{2\pi} \int_0^{2\pi} \int_{t_n}^{t_n+\tau} (z_0 S) (\tilde{Q}) d\tilde{t} d\omega, \end{aligned} \quad (4.12)$$

$$\begin{aligned} u(P) &= \frac{1}{\pi z_0(P)} \int_0^{2\pi} (-p + z_0 u \cos \theta + z_0 v \sin \theta) (Q) \cos \omega d\omega \\ &\quad + \frac{1}{\pi z_0(P)} \int_0^{2\pi} \int_{t_n}^{t_n+\tau} z_0 (c_{0x} u + c_{0y} v) (\tilde{Q}) \cos \omega d\tilde{t} d\omega \\ &\quad + \frac{1}{\pi z_0(P)} \int_0^{2\pi} \int_{t_n}^{t_n+\tau} (z_0 S) (\tilde{Q}) \cos \omega d\tilde{t} d\omega, \end{aligned} \quad (4.13)$$

with an analogous equation for v . Here $z_0 = c_0 \rho_0$ is the impedance of the medium and S is a source term

$$S := c_0 \{ u_x \sin^2 \theta - (u_y + v_x) \sin \theta \cos \theta + v_y \cos^2 \theta \}. \quad (4.14)$$

In order to derive the approximate evolution operator we firstly approximate the base of the characteristic conoid, i.e. wave front. As follows from (4.11) the geometry of the wavefront is described by the angle $\theta = \theta(\omega, t_n)$. In fact the wave front can be approximated by a circle up to second order accuracy. This allows us to evaluate spatial integrals in (4.12), (4.13) and use the technique already developed for linearized systems, cf. [11, 12, 13, 17]. To approximate a heterogeneous medium the wave speed c_0 as well as density ρ_0 are approximated by piecewise constants on a staggered grid.

Problem 3. The aim of this experiment is to illustrate capability of the FVEG method to model a wave propagation in a heterogenous medium having complex interface not aligned to the grid. The piecewise constant wave speed is defined as

$$c_0(x, y) = \begin{cases} 1.0 & \text{if } x \leq 0.5 \cos(2\pi(y - 0.4)) + 0.4 \\ 0.5 & \text{otherwise.} \end{cases}$$

The computational domain is chosen to be $[-0.95; 1.2] \times [-0.675; 1.475]$. The initial data model a circular pressure pulse

$$p(x, y) = \begin{cases} 1.0 + 0.5(\cos(\pi r/0.1) - 1.0) & \text{if } r < 0.1 \\ 0 & \text{otherwise,} \end{cases}$$

$$u(x, y) = 0 = v(x, y),$$

where the radius r is given by $r := \sqrt{(x - 0.25)^2 + (y - 0.4)^2}$. We set $\gamma = 1.0$, $p_0 = 1.0$.

In Figure 4.6 isolines of pressure are depicted at different time instances. We can clearly observe a change in the shape of circular waves as they propagate into the different medium. Moreover, due to the curved interface a complex pattern of reflected waves and their superposition can be noticed.

Acknowledgement. The research of the first author has been supported by Deutsche Forschungsgemeinschaft grant LU 1470/2-1 as well as by the 6th Framework Programme of European Union under the Contract MEST-CT-2005-021122. We would like to thank our colleagues Sebastian Noelle (Aachen), Phoolan Prasad (Bangalore), Eitan Tadmor (Maryland) and Gerald Warnecke (Magdeburg) for fruitful discussions on the topic.

References

- [1] Arun K.R., Kraft M., Lukáčová-Medviďová M., Prasad P. Finite volume evolution Galerkin method for hyperbolic conservation laws with spatially varying flux functions. *J. Comput. Physics* 2009; **228(2)**:565-590.
- [2] Barrett J.W., Morton K.W. Approximate symmetrization and Petrov-Galerkin methods for diffusion-convection problems. *Comput. Methods Appl. Mech. Engrg.* 1984; **45**: 97-122.
- [3] Brenier Y. Average multi-valued solutions for scalar conservation laws. *SIAM J. Numer. Anal.* 1984; **21**:1013-1037.
- [4] Butler D.S. The numerical solution of hyperbolic systems of partial differential equations in three independent variables. *Proc. Roy. Soc.* 1960; **255A**:233-252.

- [5] Childs P. N., Morton K.W. Characteristic Galerkin methods for scalar conservation laws in one dimension. *SIAM J. Numer. Anal.* 1990; **27**:553–594.
- [6] Kröger T., Lukáčová-Medvidová M. An evolution Galerkin scheme for the shallow water magnetohydrodynamics equations in two space dimensions. *J. Comput. Physics* 2005; **206**:122-149.
- [7] Lax P.D., Wendroff B. Systems of conservation laws. *Comm. Pure and Appl. Math.* 1960; **13**:217–237.
- [8] LeVeque R.J. *Numerical Methods for Conservation Laws*. 1992; Birkhäuser.
- [9] LeVeque R.J. *Finite Volume Methods for Hyperbolic Problems*. 2002; Cambridge University Press.
- [10] Lin P., Morton K.W., Süli E. Euler characteristic Galerkin scheme with recovery. *Math. Modelling and Numer. Anal.* 1993; **27**:863–894.
- [11] Lukáčová-Medvidová M., Morton K.W., Warnecke G. Evolution Galerkin methods for hyperbolic systems in two space dimensions. *MathComp.* 2000; **69**:1355–1384.
- [12] Lukáčová-Medvidová M., Saibertová J., Warnecke G. Finite volume evolution Galerkin methods for nonlinear hyperbolic systems. *J. Comput. Physics* 2002; **183**:533-562.
- [13] Lukáčová-Medvidová M., Morton K.W., Warnecke G. Finite volume evolution Galerkin (FVEG) methods for hyperbolic problems. *SIAM J. Sci. Comput.* 2004; **26(1)**:1-30.
- [14] Lukáčová-Medvidová M., Warnecke G., Zahaykah Y. Finite volume evolution Galerkin schemes for three-dimensional wave equation system. *Appl. Num. Math.* 2007; **57(9)**:1050-1064.
- [15] Lukáčová-Medvidová M., Warnecke G., Zahaykah Y. On the boundary conditions for EG-methods applied to the two-dimensional wave equation systems, *J. Appl. Mech. Math. (ZAMM)* 2004; **84(4)**:237-251.
- [16] Lukáčová-Medvidová M., Warnecke G., Zahaykah Y. On the stability of Evolution Galerkin schemes applied to a two-dimensional wave equation system. *SIAM J. Numer. Anal.* 2006; **44**:1556-1583.
- [17] Lukáčová-Medvidová M., Noelle S., Kraft M. Well-balanced finite volume evolution Galerkin methods for the shallow water equations. *J. Comp. Physics*, 2007; **221**:122-147.
- [18] Lukáčová-Medvidová M., Tadmor E. On the entropy stability of the Roe-type finite volume methods. *Proceedings of the twelfth international conference on hyperbolic problems*, American Mathematical Society, eds. J.-G.Liu et al., 2009.
- [19] McDonald P.W. The computation of transonic flow through two-dimensional gas turbine cascades. *ASME Proc. Paper 71-GT-89*, ASME, New York, 1971.
- [20] Morton K.W. *Numerical Solution of Convection-Diffusion Problems*, Chapman and Hall, 1996.

- [21] Morton K.W. On the analysis of finite volume methods for evolutionary problems. *SIAM J. Numer. Anal.* 1998; **35**:2195–2222.
- [22] Morton K.W. Discretization of unsteady hyperbolic conservation laws. *SIAM J. Numer. Anal.* 2001; **5**:1556–1597.
- [23] Morton K.W., Sonar T. Finite volume methods for hyperbolic conservation laws. *Acta Numerica* 2007; **16**:155–238; (A. Iserles, ed.), Cambridge University Press.
- [24] Noelle S., Pankratz N., Puppo G., Natvig J. Well-balanced finite volume schemes of arbitrary order of accuracy for shallow water flows. *J. Comput. Physics* 2006; **213**:474–499.
- [25] Ostkamp S. Multidimensional characteristic Galerkin schemes and evolution operators for hyperbolic systems. *Math. Meth. Appl. Sci.* 1997; **20**:1111–1125.
- [26] Prasad P. *Nonlinear Hyperbolic Waves in Multidimensions*. Chapman & Hall/CRC Monographs and Surveys in Pure and Applied Mathematics. 2001.
- [27] Prasad P., Ravindran R. Canonical form of a quasilinear hyperbolic system of first order equations. *J. Math. Phys. Sci.* 1984; **18(4)**: 361– 364.
- [28] Reddy A.S., Tikekar V.G., Prasad P. Numerical solution of hyperbolic equations by method of characteristics. *J. of Mathematical and Physical Sciences* 1982; **16(6)**: 575–603.
- [29] Rizzi A.W., Inouye M. Time split finite volume method for three dimensional blunt body flows. *AAIA Journal* 1973; **11**: 1478–1485.
- [30] Tadmor E. Entropy stability theory for difference approximations of nonlinear conservation laws and related time-dependent problems. *Acta Numerica* 2003; 451-512.
- [31] Tadmor E., Zhong W., Entropy stable approximation of the Navier-Stokes equations with no artificial numerical viscosity. *J. Hyperbolic. Differ. Equ* 2006; **3(3)**:529-559.

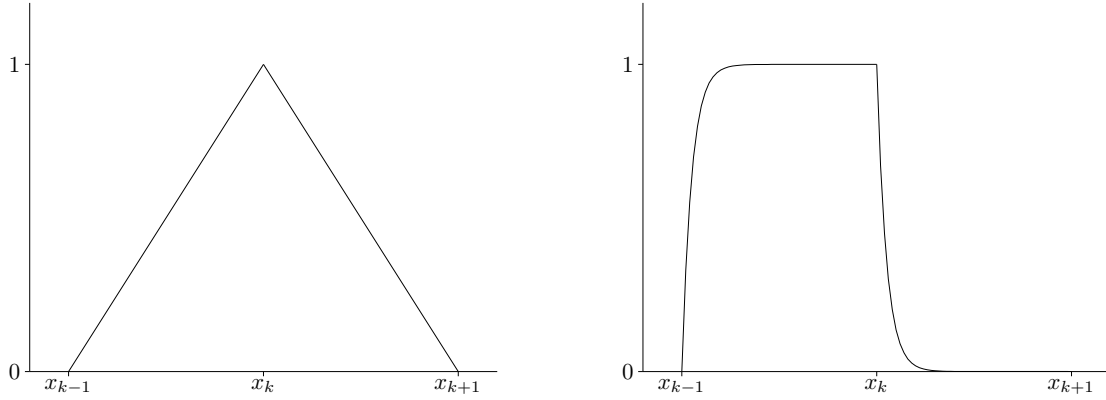


Figure 1.1: Piecewise linear test function and the Hemker test function.

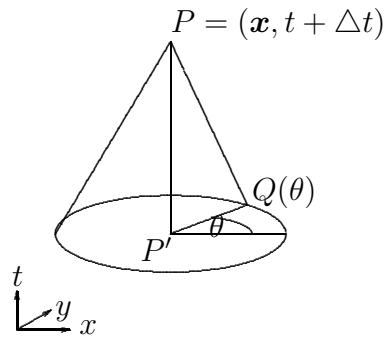


Figure 2.1: Bicharacteristics and the straight bicharacteristic cone through P and $Q(\theta)$.

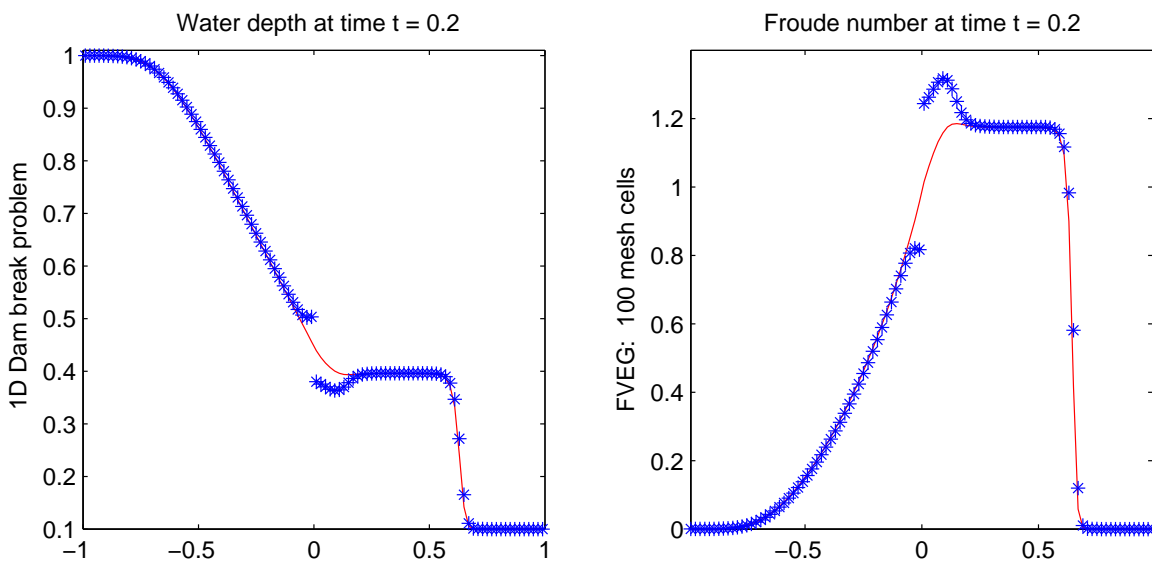


Figure 3.1: Entropy glitch problem in the first order FVEG method; results with entropy correction (solid line), without correction (stars), cf. [18].

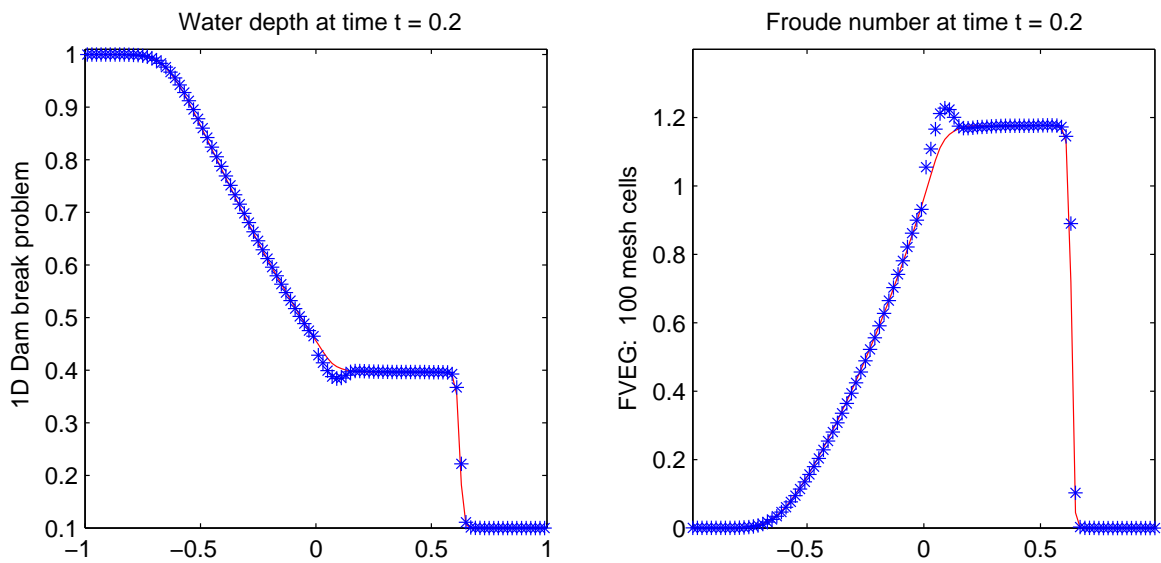


Figure 3.2: Entropy glitch problem in the second order FVEG method; results with entropy correction (solid line), without correction (stars), cf. [18].

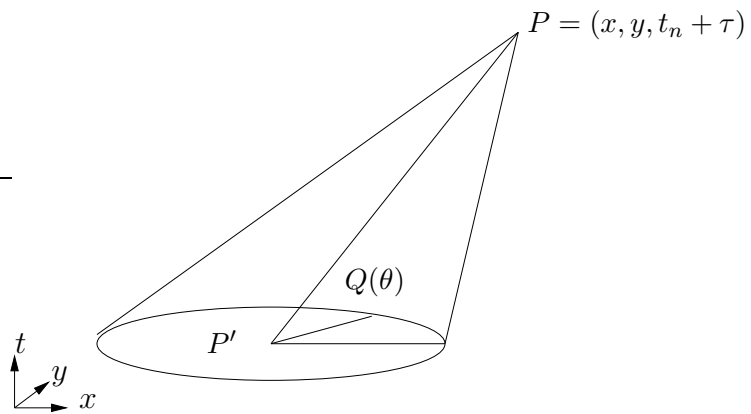


Figure 4.1: Slanted bicharacteristic cone.

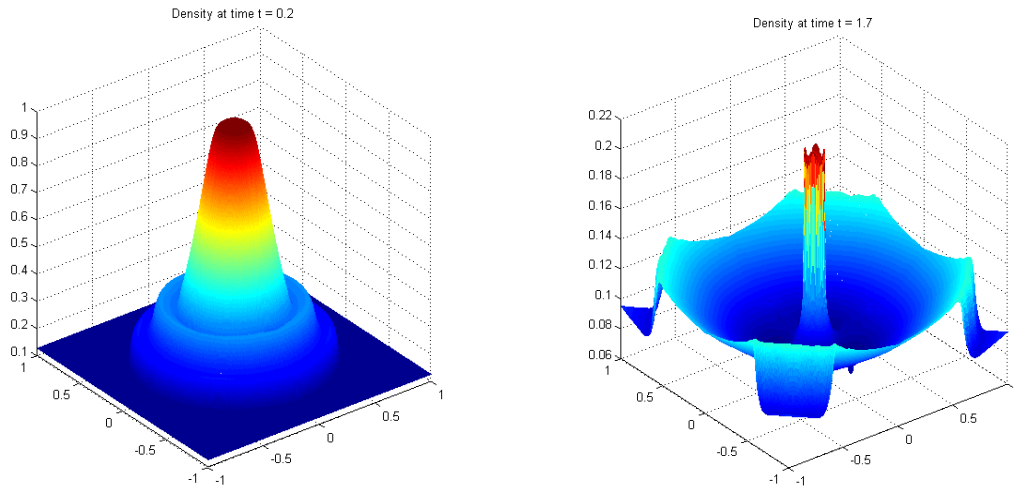


Figure 4.2: Cylindrical explosion; graphs of density at $T = 0.2$ and $T = 1.7$. Solution obtained by the FVEG scheme on a 400×400 mesh, cf. [13].

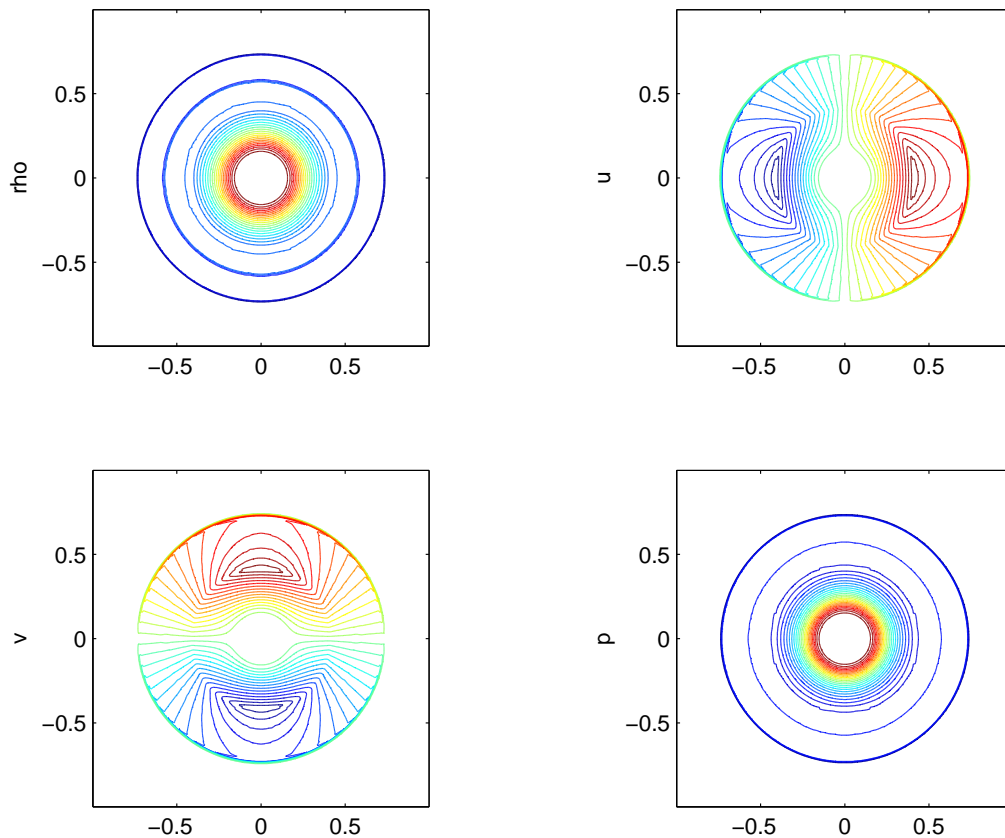


Figure 4.3: Cylindrical explosion; isolines of the solution obtained by the FVEG scheme $T = 0.2$ on a 400×400 mesh: the plots show density ρ , velocities (u, v) , and pressure p , cf. [13].

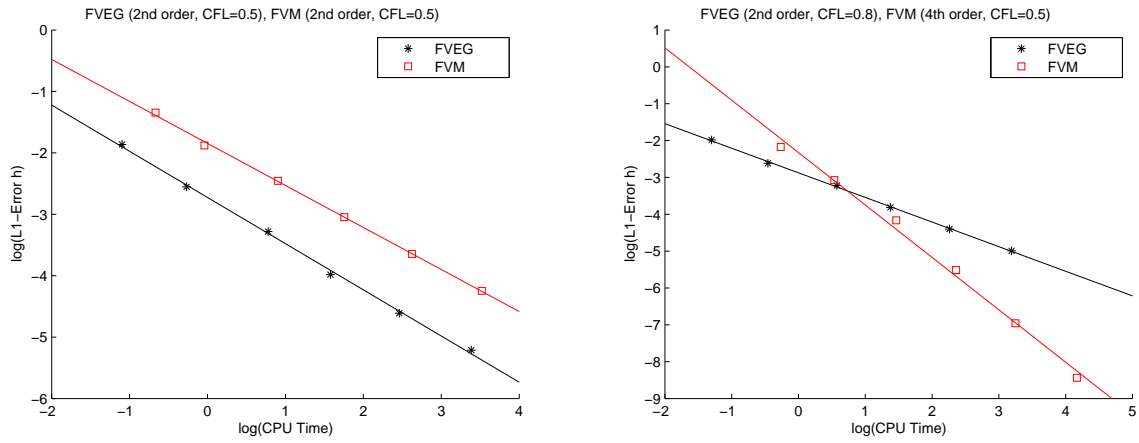


Figure 4.4: Efficiency test: L^1 error over the CPU time; the second order FVEG and second order FV schemes (left) as well as the fourth order FVM and the second order FVEG scheme (right), cf. [17].

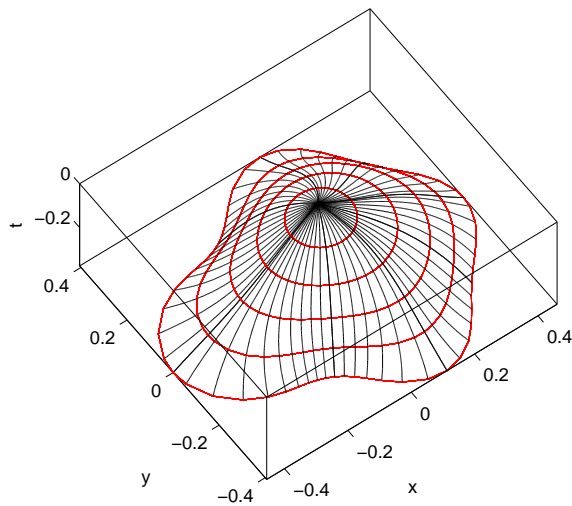


Figure 4.5: Characteristic conoid

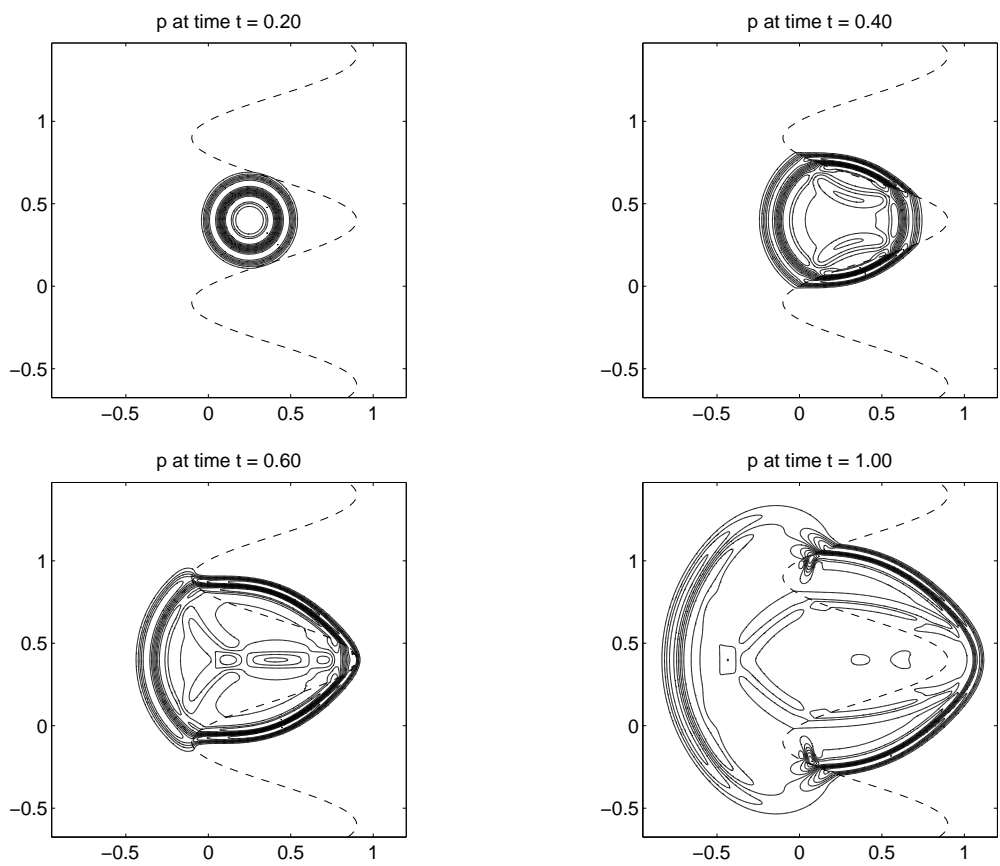


Figure 4.6: Solution isolines for p at different times, cf. [1].